15th Global Conference on Sustainable Manufacturing

Topology and shape optimization with explicit geometric constraints using a spline-based representation and a fixed grid

Yosef M. Yoely[a], Oded Amir[b,*], Iddo Hanniel[a,1]

[a]*Faculty of Mechanical Engineering, Technion – Israel Institute of Technology, Haifa 32000, Israel*
[b]*Faculty of Civil and Environmental Engineering, Technion – Israel Institute of Technology, Haifa 32000, Israel*

Abstract

Topology optimization is a computational method for finding the distribution of material such that an objective function is minimized subject to a set of constraints. In the context of structures, topology optimization aims to find the layout by changing the shape of the boundary and the number and shape of holes. Such optimized designs ultimately lead to energy savings, efficient usage of materials, and to faster and sustainable manufacturing. In this paper, we present an optimization approach that is based on explicit B-spline representation of the design, conforming with CAD standards. This parametrization enables to incorporate explicit constraints on minimum and maximum areas of holes and on curvatures of boundaries. Therefore practical design considerations such as avoiding stress concentrations in sharp corners and flexibility with respect to locations and sizes of holes can be embedded into the optimization problem. Furthermore, control of curvature can simplify machining processes leading to more efficient and sustainable manufacturing.

Keywords: Topology optimization; Shape optimization; CAD; B-splines; Explicit geometric constraints; Curvature constraints

1. Introduction

Topology optimization is a computational method for finding the distribution of material such that an objective function is minimized subject to a set of constraints. It has received considerable research attention since the pioneering work of Bendsøe and Kikuchi[3]. Various approaches have been proposed for structural topology optimization and it now has been extended to a wide range of other physical disciplines – motivated by the fact that the method can ultimately lead to energy savings, efficient usage of materials, and to faster and sustainable manufacturing. For state-of-the-art reviews of the recent developments in topology optimization, the readers are referred to [7,20] and references therein. Furthermore, basic topology optimization capabilities have recently been implemented in commercial CAD software (e.g. Inventor and NX) for solving practical design optimization problems.

The majority of existing topology optimization procedures are developed within the density-based approach. In this approach, the design domain is first discretized using finite elements with reasonable resolution. Then mathematical

---

* Corresponding author. Tel.: +972-4-829-3041 ;fax: +972-4-829-3041.
  E-mail address: odedamir@technion.ac.il (Oded Amir).

1 Currently at Mobileye, 12 Hartum st, Jerusalem, Israel.

programming algorithms and material interpolation functions [2,4] are applied to find the element-wise black-and-white density (i.e 0 or 1 in each elements) which yields the topology of structure. Although density-based methods reached remarkable achievements, there are still some challenging issues that justify further explorations. First, it is worth noting that the density-based geometry/topology representation is not quite consistent with that in current CAD systems, where the geometries/topologies of structures are often described by geometric primitives such as points, line segments or B-spline curves. Therefore topology optimization cannot be conducted directly on a CAD platform. Second, because no geometrical information is embedded in the density-based topology optimization approaches explicitly, it is difficult to provide precise control over certain structural features – for example minimum and maximum areas of holes and minimum and maximum curvatures of boundaries. These quantities are typically very important due to manufacturing considerations. Filtering and projection techniques can be utilized for imposing some of these manufacturing considerations [e.g. 11,19]. However, they typically require a large number of design iterations and constraining the geometry of specific parts is not straightforward [5].

In another leading approach – the level-set method [1,24] – the structural boundary is identified by extracting the zero contour of the level-set function. Geometry information such as the normal outward vector and curvature of the boundary can be calculated from the level-set function. Nevertheless, level-set methods basically suffer from the same disadvantage of density-based methods because of their implicit geometry representation which is too quite different from the explicit one adopted in CAD modeling systems.

This paper describes a topology optimization approach that is based on an explicit representation of the boundary using B-splines while keeping an underlying fixed grid for finite element analysis. It should be noted that this is not the first attempt to utilize B-splines on fixed grids for this purpose [8,14,15]. Other explicit representations were also suggested recently, essentially proposing direct projection of geometric entities [12,17]. Our primary aim is to establish a direct link between structural topology optimization and efficient manufacturing via CAD modeling, which enables to conduct topology optimization in a geometrically explicit manner. The main advantage of the proposed approach is in incorporating explicit geometric constraints, so that design considerations (e.g. areas of holes) and machining considerations (e.g. curvature radii of holes and boundaries) can be treated in a more flexible way than in other methods. Furthermore, it generates designs with smooth continuity boundaries that can be integrated directly into CAD. In the present work, for simulating the mechanical response we utilize the concept of fixed grid finite element analysis, which is very efficient as remeshing is not required. Nevertheless, more advanced procedures such as iso-geometric analysis (IGA,[6]) can be used in conjunction with the spline-based boundary representation.

2. B-splines and fixed grid

In this section, we will briefly review the fundamentals of B-splines and the finite element analysis that is performed on a fixed grid, according to the boundary projected from the B-splines.

2.1. B-spline and Differential geometry

B-splines and non-uniform rational B-splines (NURBS) have become the standard representation in CAD systems as they have many useful characteristics for representing domain boundaries. B-splines have a local control property and an individual control point can affect only some local part of the curve due to its formulation. A general B-spline curve is defined by (1):

$$C(t) = \sum_{i=0}^{n} N_{i,p}(t)\mathbf{P}_i \tag{1}$$

where $\mathbf{P}_i$ are the $(n+1)$ control points, $N_{i,p}(t)$ are the pth-degree B-spline basis functions, and t is the knot variable [18]. The basis functions $N_{i,p}(t)$ are defined recursively by Cox-de Boor recursion formula (2):

$$N_{i,0}(t) = \begin{cases} 0 & \text{if } t_i \le t \le t_{i+1} \\ 1 & \text{otherwise} \end{cases}$$

$$N_{i,p}(t) = \frac{t - t_i}{t_{i+p} - t_i} N_{i,p-1}(t) + \frac{t_{i+p+1} - t}{t_{i+p+1} - t_{i+1}} N_{i+1,p-1}(t) \tag{2}$$

where t_i are knot values which form the knot vector.

If the knot vector does not have any particular structure, the generated curve will not touch the first and last legs of the control polygon. In our research, a closed B-spline is implemented by forcing the first p control points to be identical to the last p control points (unclamped curve, [18]). Figure 1 shows an example of closed cubic B-spline curve with 6 control points. The control points $(P_7, \ldots, P_{10})$ are used to close the curve then: $C(t = p) = C(t = n)$.

Fig. 1. An unclamped closed cubic B-spline curve.

Green's theorem gives the relationship between a line integral around a simple closed curve and the area enclosed by the curve. In this work, we use Green's theorem to compute the area A of a closed planar parametric curve $C(t) = (x(t); y(t))$, given by (3):

$$A = \frac{1}{2} \oint_C (-x'(t)y(t) + x(t)y'(t))dt \tag{3}$$

As $C(t)$ is a parametric curve and $C'(t)$ and $C''(t)$ are its first and second derivatives, the curvature function of $C(t)$ can be computed as follows [10]:

$$\kappa(t) = \frac{(C'(t) \times C''(t))}{|C'(t)|^3} = \frac{x'y'' - y'x''}{(x'^2 + y'^2)^{3/2}} \tag{4}$$

2.2. Fixed grid finite element analysis

Finite element analysis has played a primary role in the development of CAD. Since at the early stages of a design process the topology of a structure is not fully developed, a fast means of estimating the response with an acceptable level of error is required. The fixed grid method has previously been used in problems where either the geometry or physical property of a structure change with time [13]. In this work, the fixed grid method is used to calculate the structural response that drives the optimization towards the stiffest structure. In the fixed grid approach, the mesh is constant and the actual design is superimposed on it. This means that there are elements, which lie inside, outside, or on the boundary of the structure [13–15].

Owing to the fixed grid geometry of all the finite elements, the stiffness matrix for each element is essentially fixed and depends only on its material properties – namely the elasticity modulus. For the case of inside and outside elements these properties are constant, meaning there is either no material or full solid material. For boundary elements, the properties consist of a combination of the inside and outside properties. The fixed-grid approximation then transforms the bi-material element into a homogeneous isotropic element where the material property is scaled by the function (5) of the area of material inside A_e^{mat} within that element $A_e = dx \times dy$.

$$\rho_e = \frac{A_e^{mat}}{A_e} \tag{5}$$

Elements which are completely outside the curve, are considered void with density $\rho_e = 0$, and have "zero" stiffness, i.e. $E(\rho_e) = E_{min} \approx E_{max} \cdot 10^{-6}$. Elements which are completely inside the curve, are considered solid with density $\rho_e = 1$, and have maximum stiffness, i.e. $E(\rho_e) = E_{max}$. Therefore the stiffness of a boundary elements is:

$$E(\rho_e) = E_{min} + (E_{max} - E_{min})\rho_e = E_{min} + (E_{max} - E_{min})\frac{A_e^{mat}}{A_e} \tag{6}$$

Here, we rely on material interpolation functions that are widely used in density-based approaches [2,21]. Kim et al.[13] assumed that a curve in a cell behaves as a straight line so there are three shapes of boundary cells, where the inside material can be rectangular; triangular; or trapezoidal. They showed that the error associated with the fixed

grid approximation reduces as the size of the finite element decreases. Kim and Chang[14] used Green's theorem to convert the domain integration into boundary integration, which produces a more convenient expression and gives an exact area (and area-fraction) calculation.

The algorithm we use in this work treats each finite element independently as a square cell ($dx \times dy$). The basic assumption of this algorithm is that a B-spline curve can only pass through a finite element in a limited number of ways. Because the closed curve moves in a clockwise direction, the interaction of a B-spline with a rectangular element can have a maximum of 14 different topological states [23], as shown in Figure 2. To find the B-spline intersection with the grid we use in our work a modern technique, based on Bézier clipping algorithm [16]. The advantages of this technique are its applicability to high order polynomials and the ability to find all solutions within a specified range of B-spline knots. The calculation process for boundary elements is therefore summarized as follows:

1. Determine whether the node is inside, on, or outside the curve. If all nodes are the same (cell type 13 or 14 in Figure 2), then $\rho_e = 1$ or $\rho_e = 0$ respectively.
2. Find the 1st cell type by setting the first knot t_p in the B-spline curve. According to the cell type, find the intersection points $(x, y)_{out}$ and $(x, y)_{last}$ of the curve with the two straight lines of the cell.
3. Use Equation (3) to calculate the area A_e^{mat} between the curve and the cell.
4. Calculate the area-fraction ρ_e by dividing A_e^{mat} by the cell area A_e.
5. Find the exit point from the cell based on the information: the curve moves in a clockwise direction; the 1st t in the current cell, t_{in} is known and equal to t_{out} from the previous cell; and the cell type. Set the specified range $[t_{in}, t_{last}]$ in the Bézier clipping algorithm and find the new t_{out}.
6. Use Equation (3) to calculate the area A_e^{mat} between the curve and the cell, and then calculate the area-fraction ρ_e by dividing A_e^{mat} by the cell area A_e. According to the next cell type, find the new intersection point.
7. Repeat step 5 until $t_{out} = t_{last}$ as calculated in step 2.

The above procedure is for the curve describing material (Figure 4), if the curve describes a hole then the cell's area-fraction will be $1 - \rho_e$ (Figure 5).
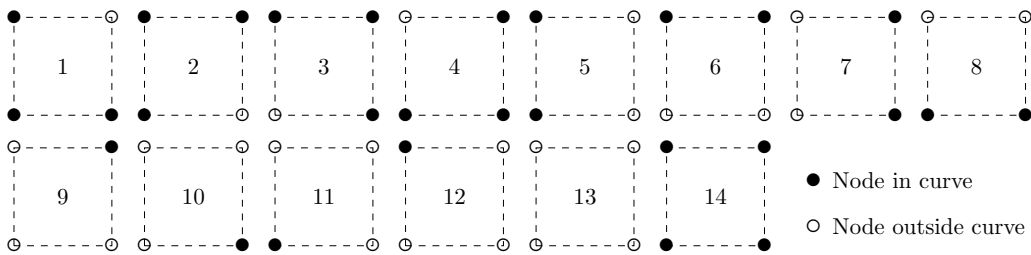

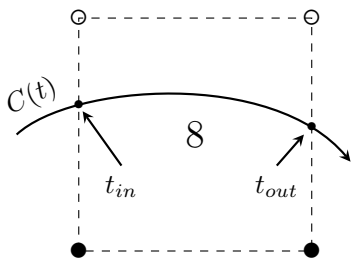Fig. 2. Cell classifications.

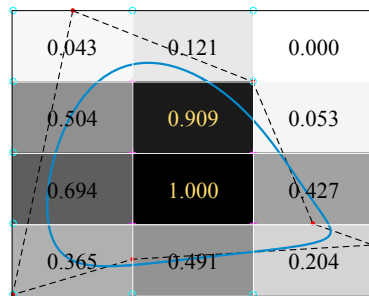Fig. 3. Example of a curve intersection with cell type 8.

Fig. 4. Example of area-fraction calculation for boundary represented by a B-spline of order 4, with 6 control points.
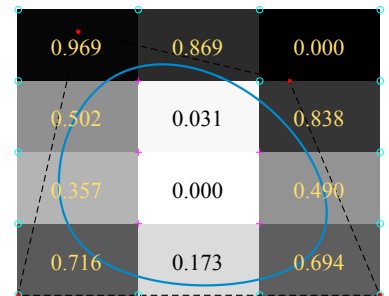
Fig. 5. Example of area-fraction calculation for hole represented by a cubic B-splines, with 4 control points.

3. Optimization problem formulation

In this work, we aim at finding the stiffest structure consisting of a boundary and holes, while constraining the areas of holes and the curvature on the boundary of the body and on the holes. This can be posed as follows:

$$\min_{\mathbf{P}} \quad f(\rho(\mathbf{P})) = \mathbf{f}^T \mathbf{u}$$

$$\text{s.t.: } g_1(\mathbf{P}) = (A_b - \sum_{i=1}^{N_h} A_h^i) - \overline{A}_p \leq 0$$

$$G_{2,i}(\mathbf{P}) = -A_h^i + \underline{A}_h^i \leq 0 \quad i = 1, .., N_h \tag{7}$$

$$G_{3,j}(\mathbf{P}) = \kappa_b^j - \overline{\kappa}_b \leq 0 \quad j = 1, .., N_{sp}$$

$$G_{4,ij}(\mathbf{P}) = -\kappa_{h,i}^j + \underline{\kappa}_{h,i} \leq 0 \quad i = 1, .., N_h \quad j = 1, .., N_{sp}$$

$$\underline{\mathbf{P}} < \mathbf{P} < \overline{\mathbf{P}} \tag{8}$$

$$\text{with: } \mathbf{K}(\rho(P))\mathbf{u} = \mathbf{f}$$

where $\mathbf{P}$ are the spatial coordinates of the control points, bounded by $\underline{\mathbf{P}}$ from below and by $\overline{\mathbf{P}}$ from above; ρ are the material densities on the fixed grid; $\mathbf{f}$ is the external forces vector; $\mathbf{u}$ is the displacements vector; i is the hole number and N_h is the number of holes; j is the curvature sampling point number and N_{sp} is the number of sampling points; A_b and A_h represent the area "inside" the closed curve in the boundary and hole(s) respectively; A_p represents the real part area $(A_b - \sum_{i=1}^{N_h} A_h^i)$; $\underline{A}$ and $\overline{A}$ are the lower and upper target areas respectively; $\underline{\kappa}$ and $\overline{\kappa}$ are the lower and upper target curvatures respectively; and $\mathbf{K}(\rho(\mathbf{P}))$ is the stiffness matrix, computed according to the densities on the finite element mesh.

In order to use gradient-based optimization algorithms for solving (7), we derive the first-order gradients of all functionals involved in the optimization, with respect to the underlying design variables, which are the coordinates $\mathbf{P}_i$ of all control points. Areas and curvatures that are involved in the various constraints can be expressed as explicit geometrical functions of the control points, based on the definition of the B-spline curves. The compliance objective however, depends on the response $\mathbf{u}$ and its derivative with respect to the control points is computed via the derivative with respect to density. These derivations are briefly reviewed in the following, where we denote a generic design variable s that can represent any coordinate x_i or y_i. Complete details regarding the derivatives can be found in Yoely[25].

For computing the derivative of the area, we use the relation given by Elber[9] who showed that when $C(t)$ is a B-spline (1), Eq. (3) can be rewritten as the bi-linear form (9):

$$2A = \begin{bmatrix} x_0, & x_1, & \ldots, & x_{n-1} \end{bmatrix} \begin{bmatrix} \phi_{0,0} & \phi_{0,1} & \cdots & \phi_{0,n-1} \\ \phi_{0,1} & \phi_{1,1} & \cdots & \phi_{1,n-1} \\ \vdots & \vdots & \ddots & \vdots \\ \phi_{n-1,0} & \phi_{n-1,1} & \cdots & \phi_{n-1,n-1} \end{bmatrix} \begin{bmatrix} y_0 \\ y_1 \\ \vdots \\ y_{n-1} \end{bmatrix} \tag{9}$$

or simply $2A = \mathbf{X}\Phi\mathbf{Y}$, where $\mathbf{X}$ and $\mathbf{Y}$ are vectors containing coordinates of $\mathbf{P_i}$, and

$$\phi_{i,j} = \oint (-N'_{i,p}(t)N_{j,p}(t) + N_{i,p}(t)N'_{j,p}(t))dt \tag{10}$$

This shows that the area is linear with respect to the control points (x_i, y_i). Furthermore, we can pre-compute all coefficients of the Φ matrix with the aid of products and integrals of B-spline functions. Then the derivative of the enclosure area in relation w.r.t. s is:

$$2A\frac{\partial A}{\partial s} = \begin{cases} \begin{bmatrix} 0, & 0, & \ldots, & 1 & \ldots, & 0 \end{bmatrix} \Phi Y & \text{if } s \in \mathbf{X} \\ X\Phi \begin{bmatrix} 0, & 0, & \ldots, & 1 & \ldots, & 0 \end{bmatrix}^T & \text{if } s \in \mathbf{Y} \end{cases} \tag{11}$$

The derivative of the curvature $\kappa(t)$ given by Eq. (4) can also be obtained by direct differentiation. However, it is much more cumbersome and requires symbolic computations that are omitted from this text for the sake of brevity.

For obtaining the derivative of f with respect to a certain design variable s which can represent any coordinate of $\mathbf{P}_i = (x_i, y_i)$, we use the chain rule:

$$\frac{\partial f}{\partial s} = \frac{\partial f}{\partial \rho_e} \frac{\partial \rho_e}{\partial s} \tag{12}$$

It should be noted that all solid and void elements do not have a dependency of their ρ_e on s because they do not intersect the curve. From density-based topology optimization, it is well known that the derivative of compliance with respect to the element density is given by equation (13):

$$\frac{\partial f}{\partial \rho_e} = -\mathbf{u}_e^T \frac{\partial \mathbf{K}_e}{\partial \rho_e} \mathbf{u}_e. \tag{13}$$

Using standard density-based topology optimization representations, we have:

$$\frac{\partial \mathbf{K}_e}{\partial \rho_e} = \frac{\partial E(\rho_e)}{\partial \rho_e} \mathbf{K}_0 = (E_{max} - E_{min})\mathbf{K}_0 \tag{14}$$

where $\mathbf{K}_0$ is the element stiffness matrix corresponding to $E = 1$.

Following Eq. (27) in Kim and Chang[14], we compute the variation of the area-fraction of a cell cut by a B-spline curve:

$$\delta\rho_e = \frac{1}{A_e} \int_C \mathbf{V}^T \mathbf{n} dt \tag{15}$$

where the boundary B-spline curve $C(t)$ is perturbed in the direction of the design velocity $\mathbf{V}$ and $\mathbf{n}$ is the outward unit normal vector to the boundary $\mathbf{n} = \frac{C'(t)}{|C'(t)|}$. From Silva and Bittencourt[22] we see that:

$$\mathbf{V}_i(t) = \frac{\partial C(t)}{\partial s} = N_{i,p}(t) \tag{16}$$

Placing equations (13) and (15) in (12) gives us the analytical expression for the sensitivity analysis of compliance:

$$\frac{\partial f}{\partial s} = -\mathbf{u}_e^T \frac{\partial \mathbf{K}_e}{\partial \rho_e} \mathbf{u}_e \frac{1}{A_e} \int_{c(t)} \mathbf{V}^T \mathbf{n} dt \tag{17}$$

4. Numerical Examples

In this section, we present several numerical examples that demonstrate the capabilities of the proposed computational approach. The optimization problem is solved using a Sequential Linear Programming (SLP) strategy. In all examples below, the main optimization loop is terminated if the change in the compliance objective is below 1%.

We first examine the design of a cantilever where the load is applied vertically in the lower right corner and the left edge is supported, see Figure 6. The design domain is assumed to be rectangular and is discretized by a grid containing 32×20 square finite elements ($dx = dy = 1.0$).

In this example we used two cubic B-splines ($p = 3$) to describe the boundary and the holes. The boundary is based on 3 moving control points, one hole ($N_h = 1$) is represented by 6 moving control points, and $N_{sp} = 100 \cdot (t_n - t_p)$. Control points can move ($0 < P_x < \texttt{nelx}$) and ($0 < P_y < \texttt{nelx}$). The part's area constraint is $\overline{A}_p = 256$ that corresponds to 40% of the bounding rectangle. Finally, the SLP move limit that determines the maximum change between design iterations is set according to the iteration number, $4/Iter^{0.9}$. Results with various values of the area and curvature constraints are presented in Figures 9 through 14.

The second example is the design of a half "MBB-beam" where the load is applied vertically in the upper left corner and there are symmetric boundary conditions along the left edge, see Figure 15. The design domain is again rectangular and is discretized by a grid containing 60×20 square finite elements ($dx = dy = 1.0$).

We again used cubic B-splines ($p = 3$) to describe the boundary and the holes. The boundary is based on 4 moving control points, the holes ($N_h = 2$) are represented by 6 moving control points, and $N_{sp} = 100 \cdot (t_n - t_p)$. Control points can move ($0 < P_x < \texttt{nelx}$) and ($0 < P_y < \texttt{nelx}$). The part's area constraint is $\overline{A}_p = 480$ that corresponds to 40% of the bounding rectangle. The SLP move limit is the same as before. Results with various values of the area and curvature constraints are presented in Figures 17 through 20.
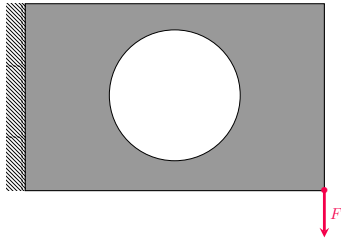
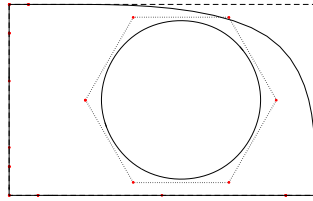Fig. 6. Design domain of the cantilever example.

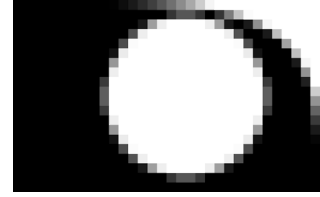
Fig. 7. Initial domain represented by B-splines.

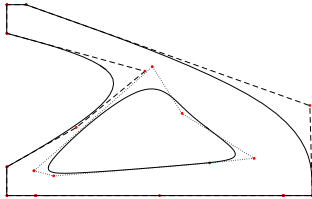Fig. 8. Initial domain represented by density on a fixed grid.

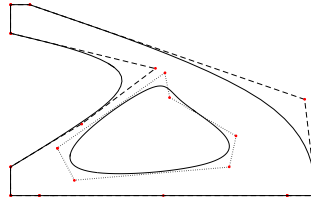
Fig. 9. Optimized design with hole curvature constraint $\underline{\kappa}_h = -3$.

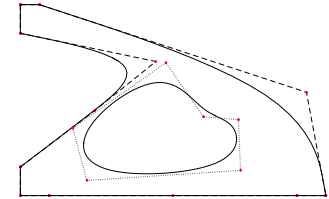Fig. 10. Optimized design with hole curvature constraint $\underline{\kappa}_h = -1$.

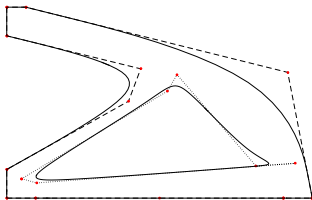Fig. 11. Optimized design with hole curvature constraint $\underline{\kappa}_h = 0.5$.

Fig. 12. Optimized design with hole area constraint $\underline{A}_h = 120$.
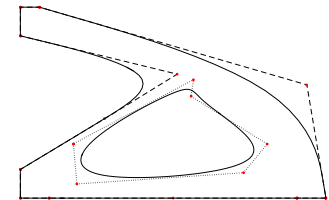

Fig. 13. Optimized design with hole area constraint $\underline{A}_h = 150$.

Fig. 14. Optimized design with hole area constraint $\underline{A}_h = 110$, boundary and hole's curvature constraints $\overline{\kappa}_b = 1$ and $\underline{\kappa}_h = 1$.
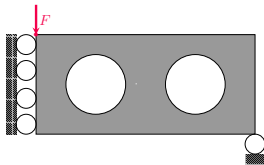

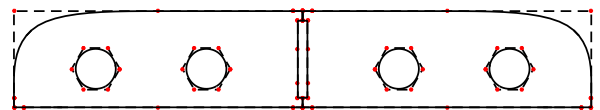Fig. 15. MBB-beam half design domain with symmetry boundary conditions.

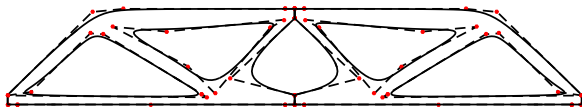Fig. 16. MBB-beam with two holes represented by B-splines.
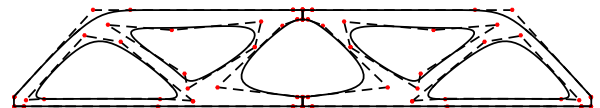

Fig. 17. MBB area constraint.

Fig. 18. MBB Boundary and holes curvature constraint $|\kappa| = 2$.

5. Conclusions and future work

In this paper, we presented a shape and topology optimization procedure with explicit geometric constraints on areas and curvatures. The method can lead to optimized layouts that reduce material usage and are tailored to specific machining parameters – hence contributing to the overall sustainability of the manufacturing process. The design is parametrized using B-splines while FEA is based on a projection of the shape upon a fixed grid so remeshing is not necessary. The proposed approach enables flexibility with respect to areas of holes and direct control over curvatures, two capabilities that are not easy to achieve in widespread density-based and level-set approaches. As a consequence, both manufacturing limitations (e.g. in the context of machining) and design limitations (e.g. stress concentrations)
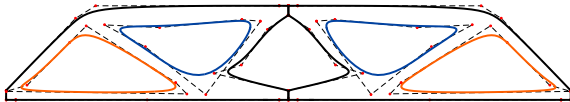
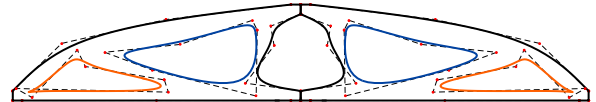Fig. 19. Min hole area $\underline{A}_h$ = 200 (Blue holes).

Fig. 20. Max hole area $\overline{A}_h$ = 100 (Orange holes).

can be considered within the design optimization. In future work, the proposed approach will be extended to enable creating and merging holes during the optimization process. Another goal will be to add control over distances between holes and between the boundary and adjacent holes.

Acknowledgements

References

[1] G. Allaire, F. Jouve, and A.-M. Toader. Structural optimization using sensitivity analysis and a level-set method. *Journal of computational physics*, 194(1):363–393, 2004.

[2] M. P. Bendsøe. Optimal shape design as a material distribution problem. *Structural optimization*, 1(4):193–202, 1989.

[3] M. P. Bendsøe and N. Kikuchi. Generating optimal topologies in structural design using a homogenization method. *Computer methods in applied mechanics and engineering*, 71(2):197–224, 1988.

[4] M. P. Bendsøe and O. Sigmund. Material interpolation schemes in topology optimization. *Archive of applied mechanics*, 69(9):635–654, 1999.

[5] A. Clausen, N. Aage, and O. Sigmund. Topology optimization with flexible void area. *Structural and Multidisciplinary Optimization*, 50(6): 927–943, 2014.

[6] J. A. Cottrell, T. J. Hughes, and Y. Bazilevs. *Isogeometric analysis: toward integration of CAD and FEA*. John Wiley & Sons, 2009.

[7] J. D. Deaton and R. V. Grandhi. A survey of structural and multidisciplinary continuum topology optimization: post 2000. *Structural and Multidisciplinary Optimization*, 49(1):1–38, 2014.

[8] C. S. Edwards, H. A. Kim, and C. J. Budd. Smooth boundary based optimisation using fixed grid. In *7th world congress on structural and multidisciplinary optimization*. University of Bath, 2007.

[9] G. Elber. Linearizing the area and volume constraints. techreport cis-2000-04, Technion - Israel Institute of Technology, 2000.

[10] R. T. Farouki and C. A. Neff. Analytic properties of plane offset curves. *Computer Aided Geometric Design*, 7(1-4):83–99, 1990.

[11] J. K. Guest and M. Zhu. Casting and milling restrictions in topology optimization via projection-based algorithms. In *ASME 2012 International Design Engineering Technical Conferences and Computers and Information in Engineering Conference*, pages 913–920. American Society of Mechanical Engineers, 2012.

[12] X. Guo, W. Zhang, J. Zhang, and J. Yuan. Explicit structural topology optimization based on moving morphable components (mmc) with curved skeletons. *Computer Methods in Applied Mechanics and Engineering*, 310:711–748, 2016.

[13] H. Kim, M. García, O. Querin, G. Steven, and Y. Xie. Introduction of fixed grid in evolutionary structural optimisation. *Engineering Computations*, 17(4):427–439, 2000.

[14] N. H. Kim and Y. Chang. Eulerian shape design sensitivity analysis and optimization with a fixed grid. *Computer methods in applied mechanics and engineering*, 194(30):3291–3314, 2005.

[15] S. Lee, B. M. Kwak, and I. Y. Kim. Smooth boundary topology optimization using b-spline and hole generation. *International journal of CAD/CAM*, 7(1), 2009.

[16] K. Mørken and M. Reimers. An unconditionally convergent method for computing zeros of splines and polynomials. *Mathematics of computation*, 76(258):845–865, 2007.

[17] J. Norato, B. Bell, and D. Tortorelli. A geometry projection method for continuum-based topology optimization with discrete elements. *Computer Methods in Applied Mechanics and Engineering*, 293:306–327, 2015.

[18] L. Piegl and W. Tiller. *The NURBS book*. Springer Science & Business Media, 2012.

[19] O. Sigmund. Morphology-based black and white filters for topology optimization. *Structural and Multidisciplinary Optimization*, 33(4): 401–424, 2007.

[20] O. Sigmund and K. Maute. Topology optimization approaches. *Structural and Multidisciplinary Optimization*, 48(6):1031–1055, 2013.

[21] O. Sigmund and S. Torquato. Design of materials with extreme thermal expansion using a three-phase topology optimization method. *Journal of the Mechanics and Physics of Solids*, 45(6):1037–1067, 1997.

[22] C. Silva and M. Bittencourt. Velocity fields using nurbs with distortion control for structural shape optimization. *Structural and Multidisciplinary Optimization*, 33(2):147–159, 2007.

[23] M. Victoria, P. Martí, and O. M. Querin. Topology design of two-dimensional continuum structures using isolines. *Computers & Structures*, 87(1):101–109, 2009.

[24] M. Y. Wang, X. Wang, and D. Guo. A level set method for structural topology optimization. *Computer methods in applied mechanics and engineering*, 192(1):227–246, 2003.

[25] Y. M. Yoely. Spline-based topological optimization with curvature constraints. Master's thesis, Technion - Israel Institute of Technology, 2017.